Supplementary Materials for

Structural basis for antibiotics murepavadin and thanatin targeting the lipopolysaccharide insertase LptD

Authors

Philippe A. Lehner[1], Laetitia Rožić[1], Seyed Majed Modaresi[1, 2], Kristyna Pluhackova[3], Peter Zbinden[4], Daniel Obrecht[4], Jaroslaw Sedzicki[1]*, Sebastian Hiller[1]*

This PDF file includes:

Figs. S1–S12

Tables S1–S3

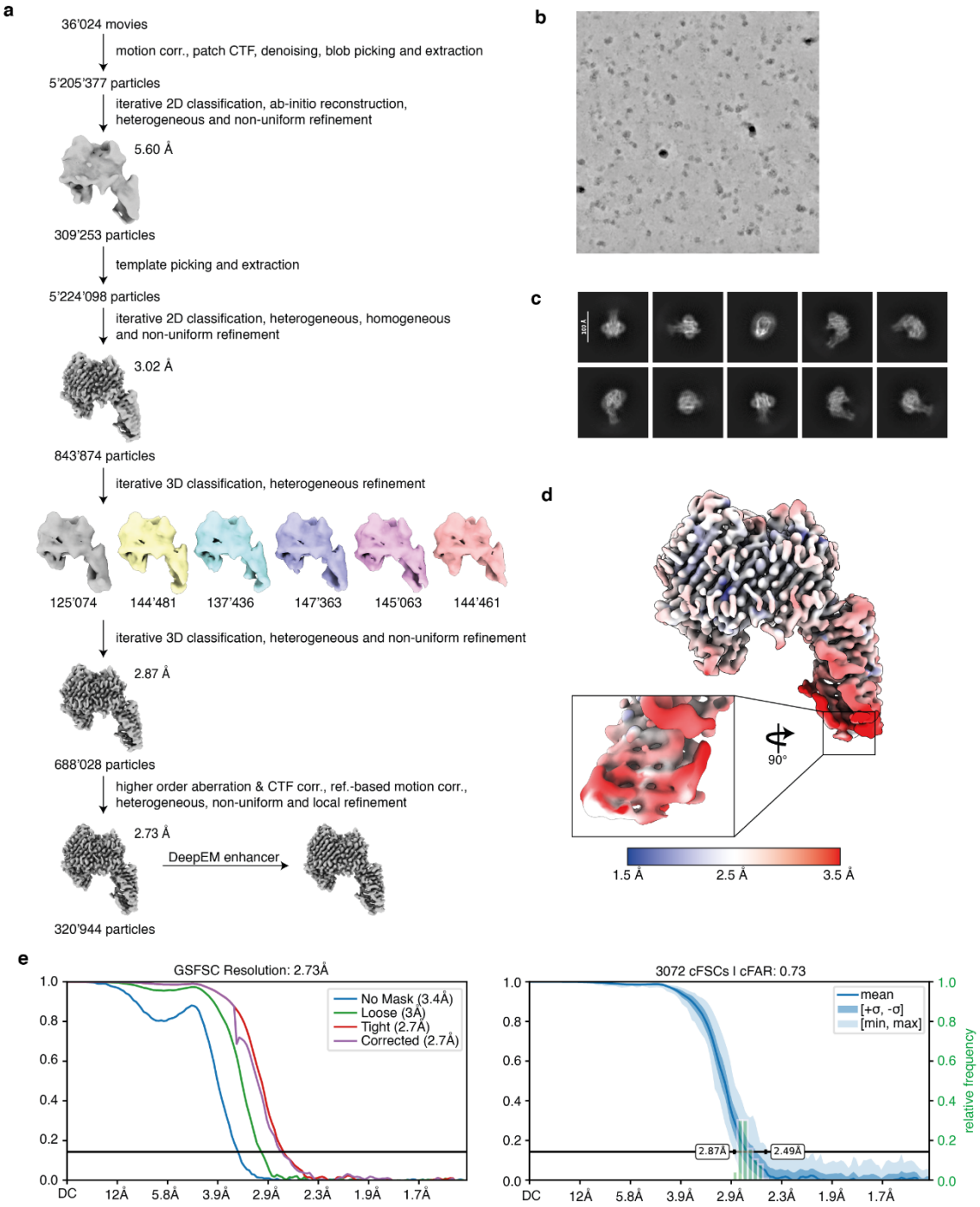

Fig. S1. Cryo-EM data processing of LptDEM$_{Eco}$-thanatin. **a** Schematic overview of the processing workflow. See Materials and Methods for details. **b** Representative example of a denoised micrograph. **c** Representative example classes that were selected during iterative 2D classification. **d** Local resolution map (red: low-resolution, blue: high-resolution) with a close-up of the distal LptD β-jellyroll domain with thanatin bound. **e** Gold-standard Fourier shell correlation (GSFSC) curve and conical Fourier shell correlation (cFSC) | conical FSC area ratio (cFAR) plot.

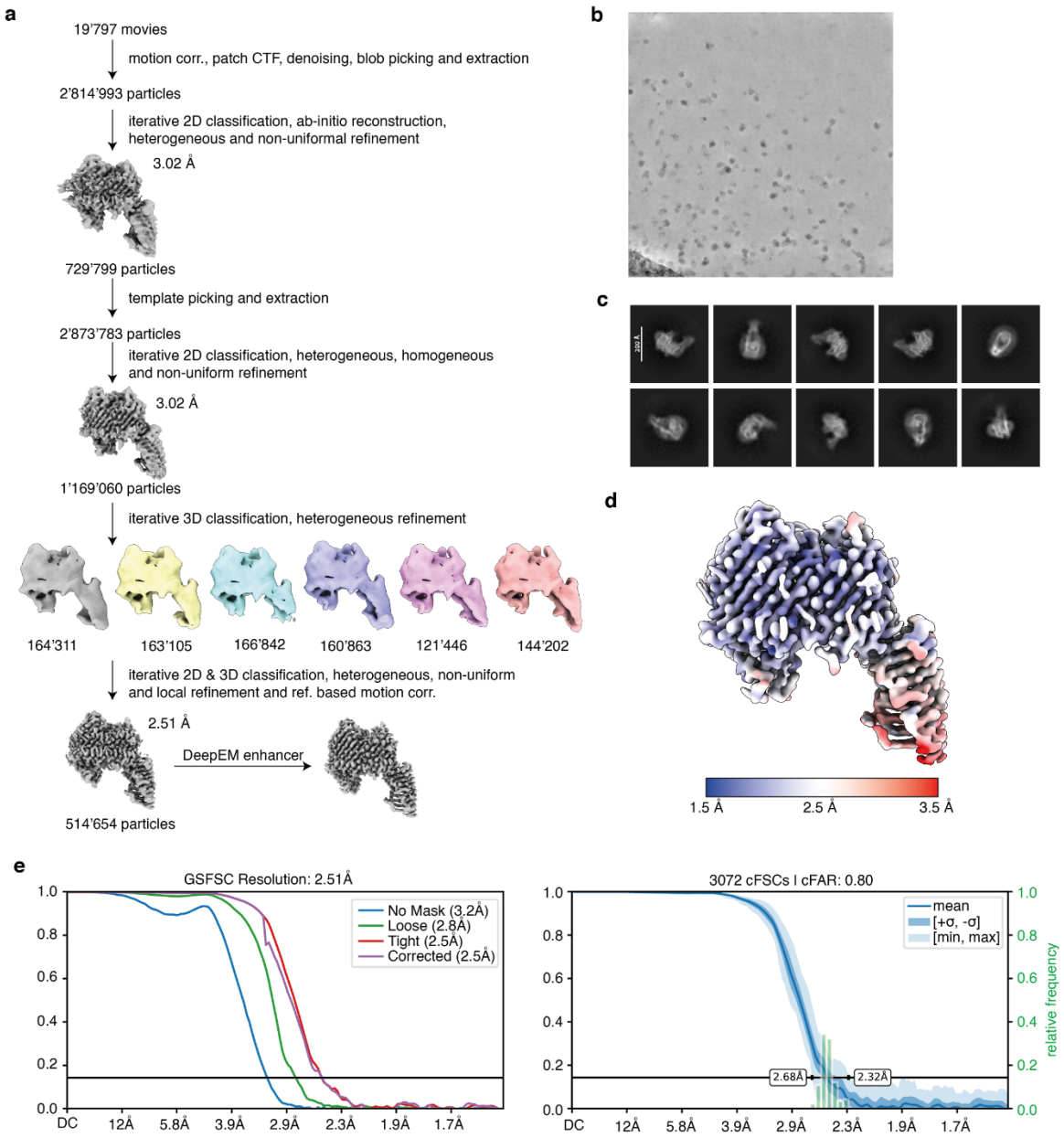

Fig. S2. Cryo-EM data processing of apo LptDEM$_{Eco}$. a Schematic overview of the processing workflow. See Materials and Methods for details. **b** Representative example of a denoised micrograph. **c** Representative example classes that were selected during iterative 2D classification. **d** Local resolution map (red: low-resolution, blue: high-resolution). **e** Gold-standard Fourier shell correlation (GSFSC) curve and conical Fourier shell correlation (cFSC) | conical FSC area ratio (cFAR) plot.

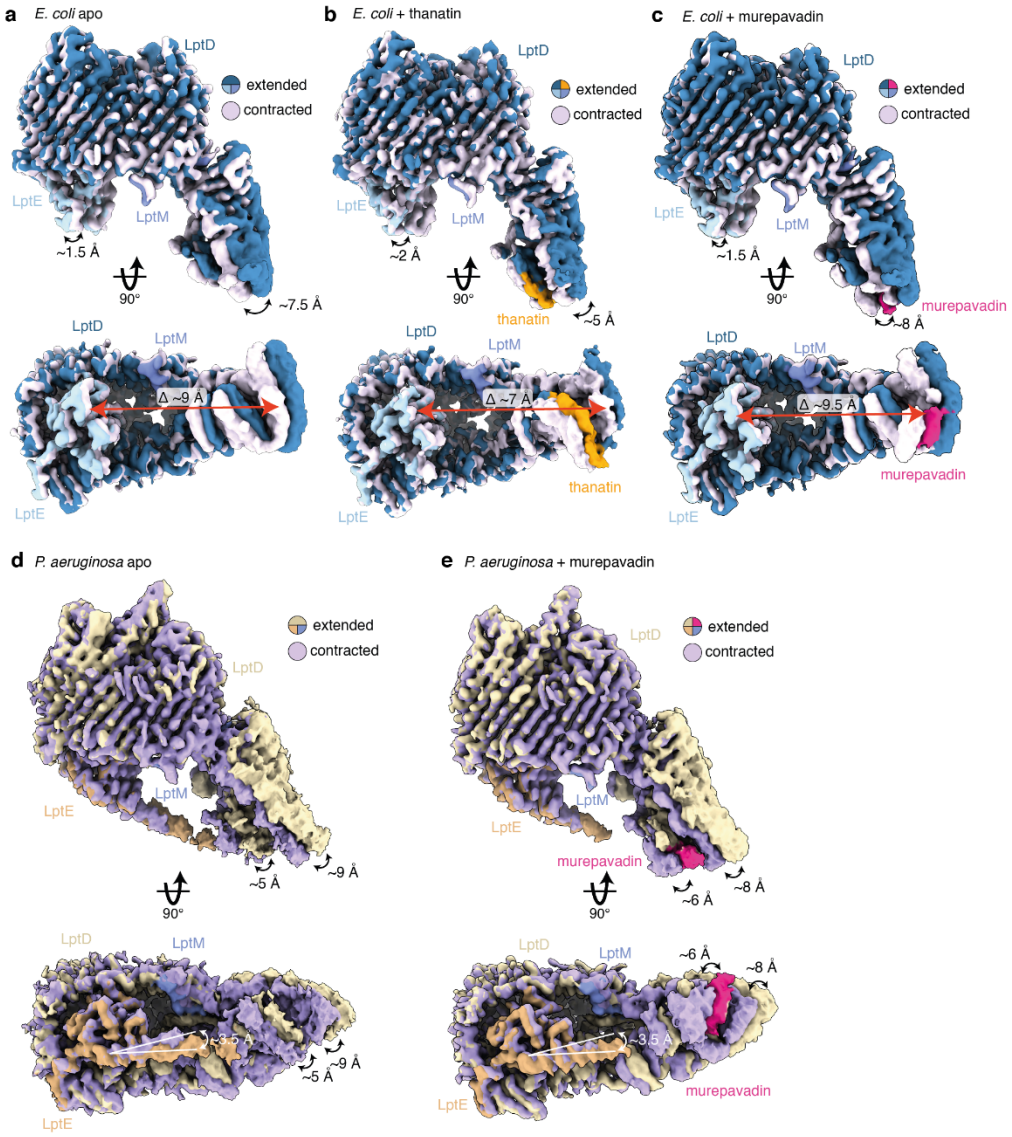

Fig. S3. 3D variability analysis of the LptDEM complexes. Overlays of the most extended (color coding according to previous LptDEM complex) and contracted (lavender) densities from 3D variability analysis in the side-view (top) and bottom view (bottom), with the largest conformational change indicated by arrows. **a** Apo LptDEM$_{Eco}$ showing approx. 1.5 Å change in LptE and 7.5 Å in the β-jellyroll domain, resulting in a relative change between the two domains of approx. 9 Å. **b** LptDEM$_{Eco}$–thanatin showing approx. 2 Å change in LptE and 5 Å in the β-jellyroll domain, resulting in a relative change between the two domains of approx. 7 Å. **c** LptDEM$_{Eco}$–murepavadin showing approx. 1.5 Å change in LptE and 8 Å in the β-jellyroll domain, resulting in a relative change between the two domains of approx. 9.5 Å. **d** Apo LptDEM$_{Pae}$ showing approx. 5 Å and 9 Å change at the distal β-jellyroll terminus as well as a 3.5 Å displacement of the periplasmic LptE helix at the farthest point resolved. **e** LptDEM$_{Pae}$–murepavadin showing approx. 6 Å and 8 Å change at the distal β-jellyroll terminus as well as a 3.5 Å displacement of the periplasmic LptE helix at the farthest point resolved.

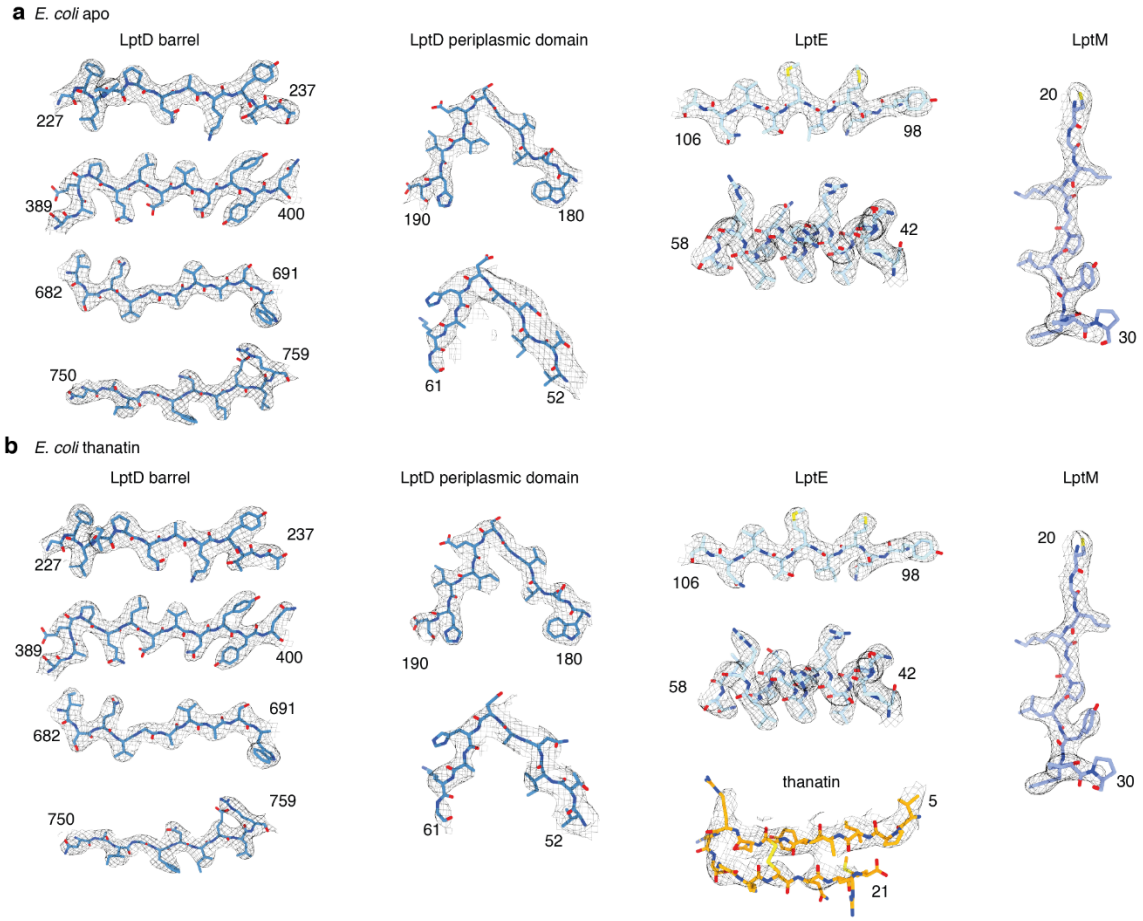

Fig. S4. Structural models of LptDEM$_{Eco}$ with and without thanatin. Representative examples of each chain of the model (LptD, LptE, LptM and ligand) at different regions of the structures, with the first and last amino acid number labeled, shown individually within the experimentally determined cryo-EM map (grey mesh) at appropriate contour levels of **a** apo LptDEM$_{Eco}$ and **b** LptDEM$_{Eco}$–thanatin.

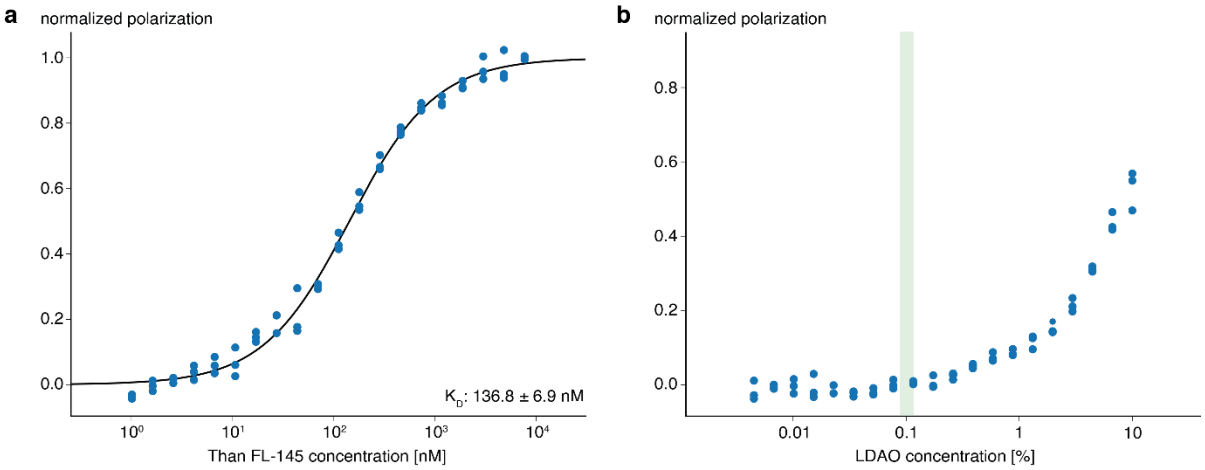

Fig. S5. Affinity determinations of thanatin. a Direct fluorescence polarization assay of fluorescently labeled thanatin (Than FL-145, fluorophore: Alexa Fluor 647) binding to $LptDEM_{Eco}$. Experimental data are shown as dots and the non-linear fit to the data as solid line, with the resulting K_D indicated. **b** Direct fluorescence polarization assay of LDAO binding to fluorescently labeled thanatin. The concentration of LDAO in the $LptDEM_{Eco}$ sample is shown in green. This control thus shows that the binding observed in (a) is not due to detergent binding.

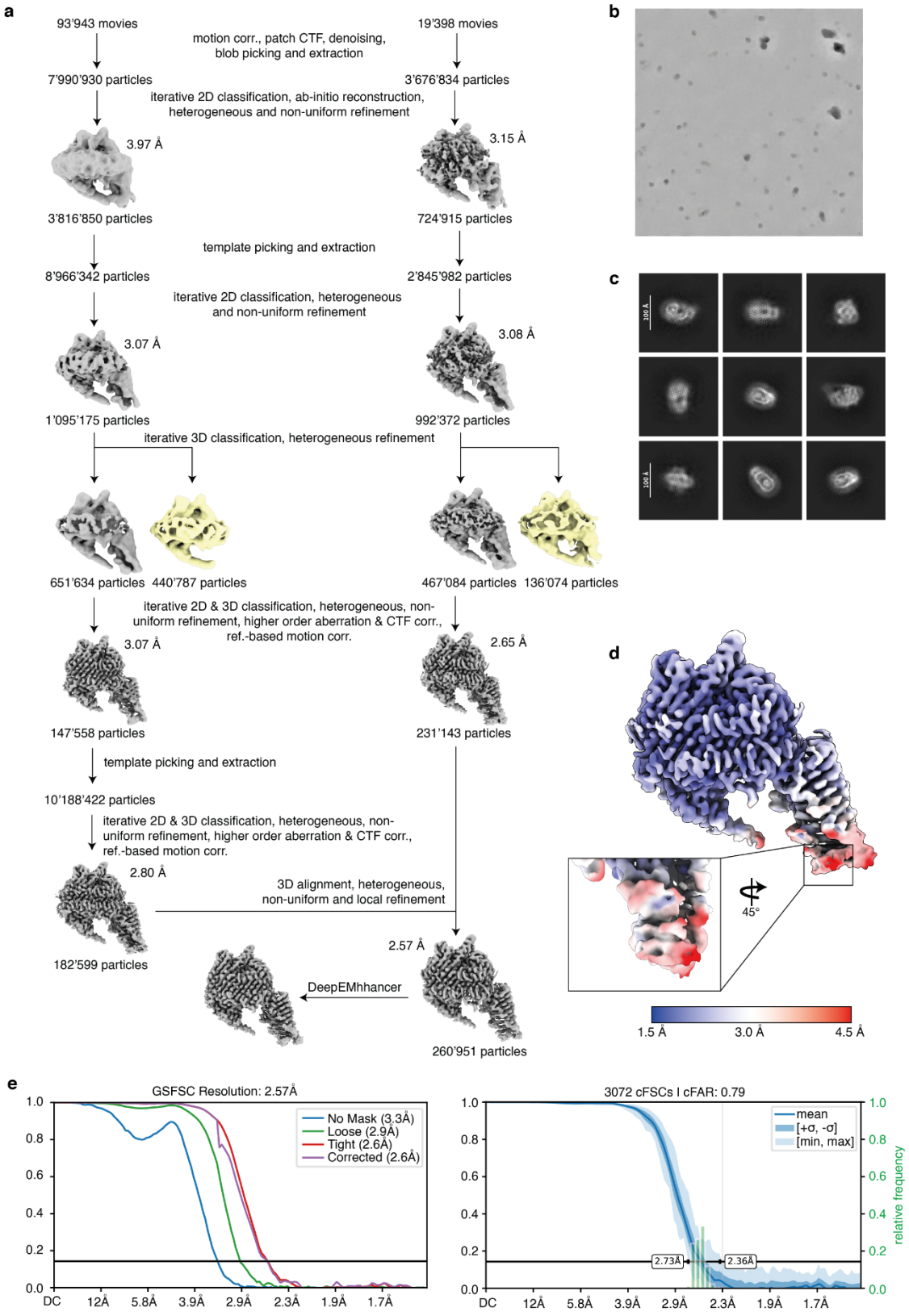

Fig. S6. Cryo-EM data processing of LptDEM$_{Pae}$-murepavadin. a Schematic overview of the processing workflow. See Materials and Methods for details. **b** Representative example of a denoised micrograph. **c** Representative example classes that were selected during iterative 2D

classification. **d** Local resolution map (red: low-resolution, blue: high-resolution) with a close-up of the distal LptD β-jellyroll domain with murepavadin bound. **e** Gold-standard Fourier shell correlation (GSFSC) curve and conical Fourier shell correlation (cFSC) | conical FSC area ratio (cFAR) plot.

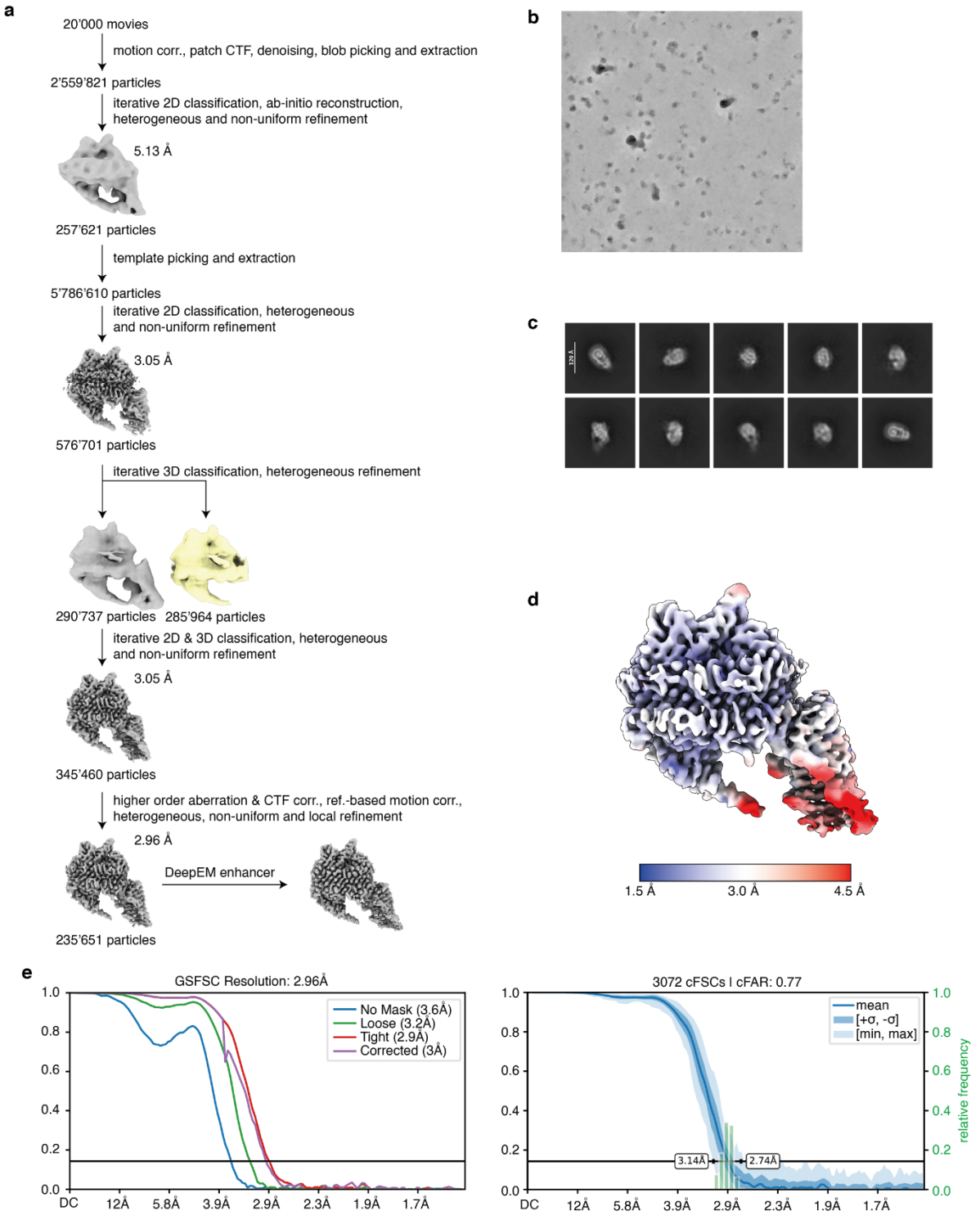

Fig. S7. Cryo-EM data processing of apo LptDEM$_{Pae}$. a Schematic overview of the processing workflow. See Materials and Methods for details. **b** Representative example of a denoised micrograph. **c** Representative example classes that were selected during iterative 2D classification. **d** Local resolution map (red: low-resolution, blue: high-resolution). **e** Gold-standard Fourier shell correlation (GSFSC) curve and conical Fourier shell correlation (cFSC) | conical FSC area ratio (cFAR) plot.

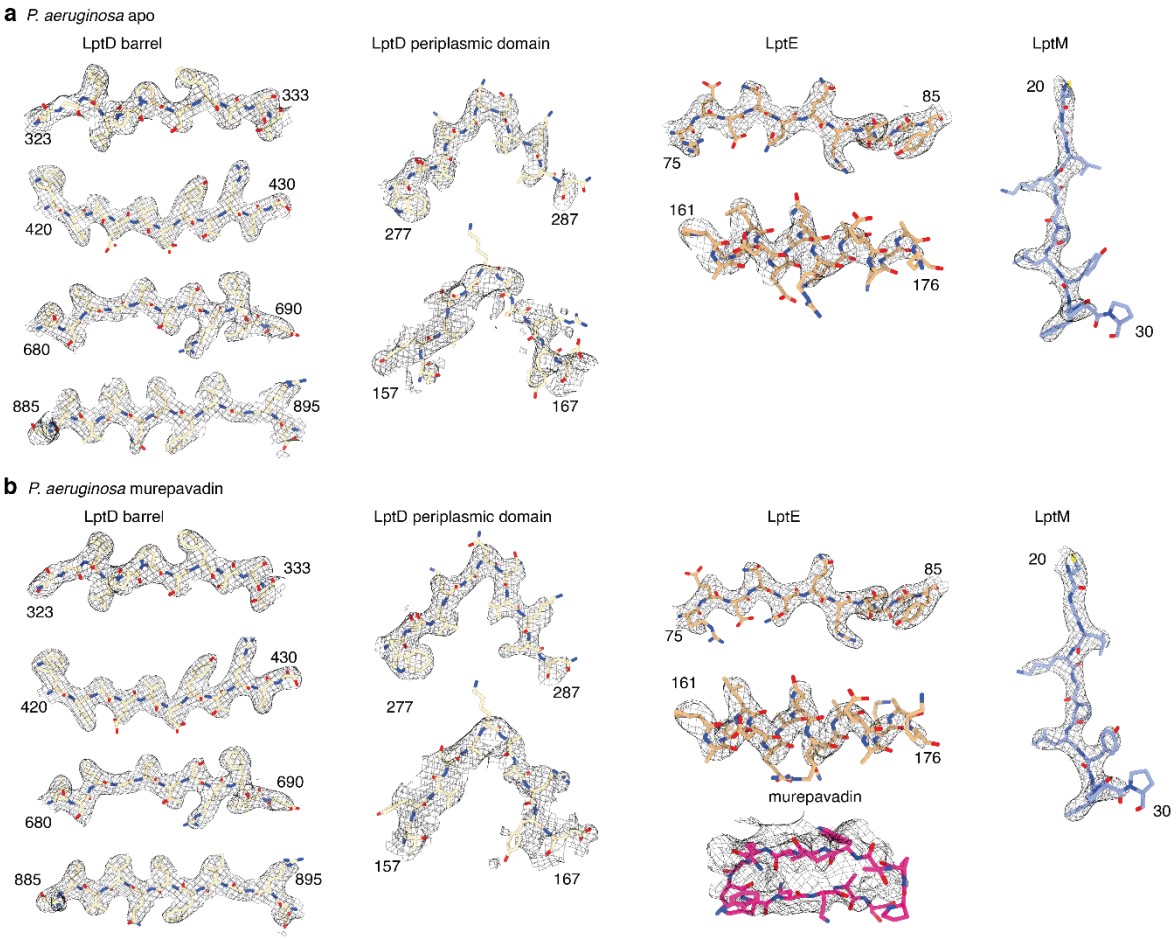

Fig. S8. Structural models of LptDEM$_{Pae}$ apo and with murepavadin. Representative examples of each chain of the model (LptD, LptE, LptM and murepavadin) at different regions of the structures, with the first and last amino acid number labeled, shown individually within the experimentally determined cryo-EM map (grey mesh) at appropriate contour levels of **a** apo LptDEM$_{Pae}$ and **b** LptDEM$_{Pae}$–murepavadin.

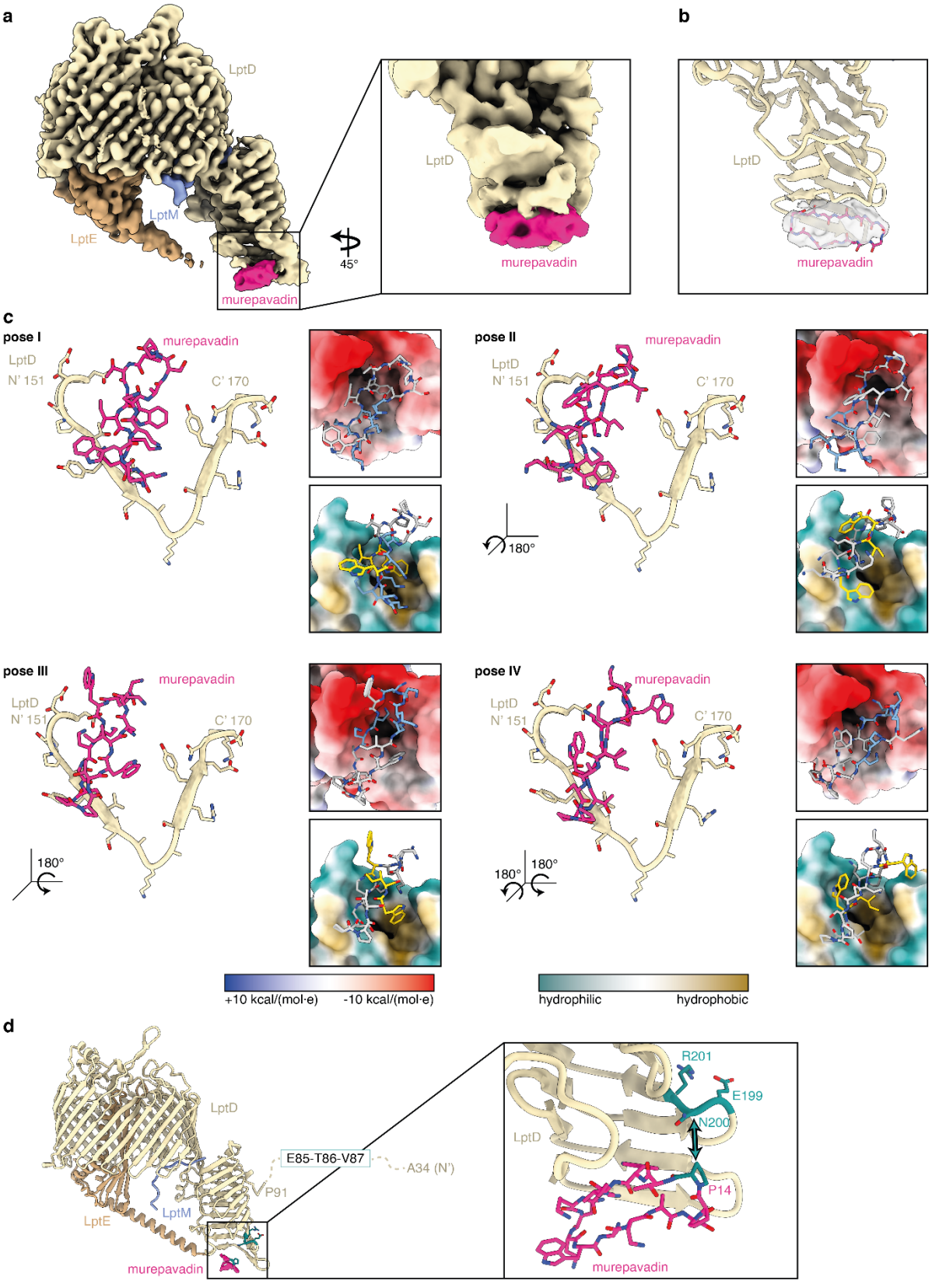

Fig. S9. Molecular poses of murepavadin binding to LptDEM$_{Pae}$. a Cryo-EM reconstructions of LptDEM$_{Pae}$–murepavadin, at representative contour levels for each subunit (LptDE$_{Pae}$, beige; LptM$_{Eco}$, blue; murepavadin, pink), with a close-up view of the density attributed to murepavadin. **b** Molecular model showing the possible backbone fit of murepavadin within its density (grey). **c**

Bottom view of the binding site with the four formally possible poses of murepavadin (I–IV). Each pose is shown in context of electrostatics and hydrophobicity of LptD, with highlighted positively charged residues (blue) or hydrophobic residues (yellow) of murepavadin. **d** Structure of $LptDEM_{Pae}$ with bound murepavadin. Residues E199–R201 of LptD, and Pro14 of murepavadin, which have previously been shown to be in close contact by chemical cross-linking are shown in turquoise.

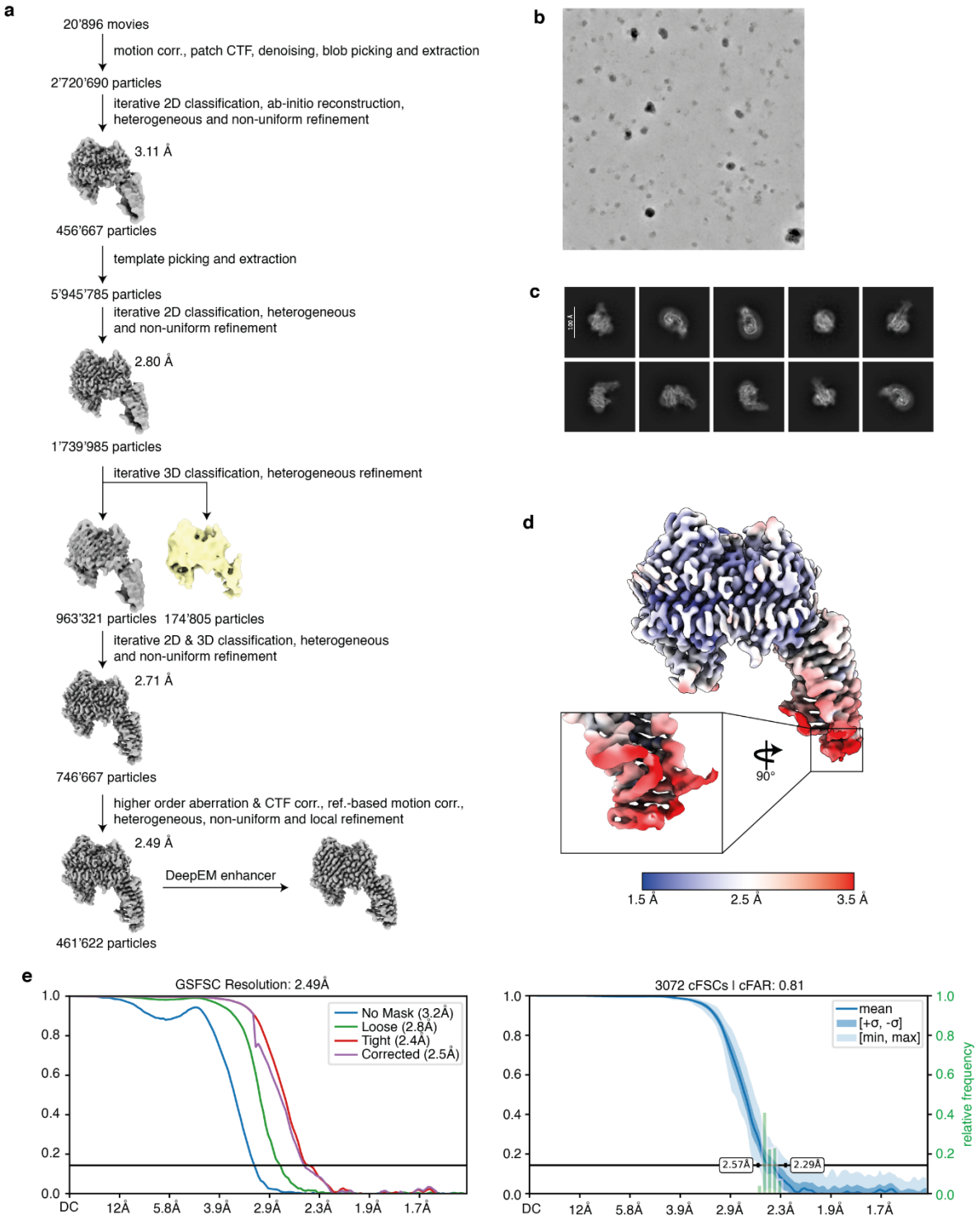

Fig. S10. Cryo-EM data processing of LptDEM$_{Eco}$–murepavadin. a Schematic overview of the processing workflow. See Materials and Methods for details. **b** Representative example of a denoised micrograph. **c** Representative example classes that were selected during iterative 2D classification. **d** Local resolution map (red: low-resolution, blue: high-resolution) with a close-up of the distal LptD β-jellyroll domain with murepavadin bound. **e** Gold-standard Fourier shell correlation (GSFSC) curve and conical Fourier shell correlation (cFSC) | conical FSC area ratio (cFAR) plot.

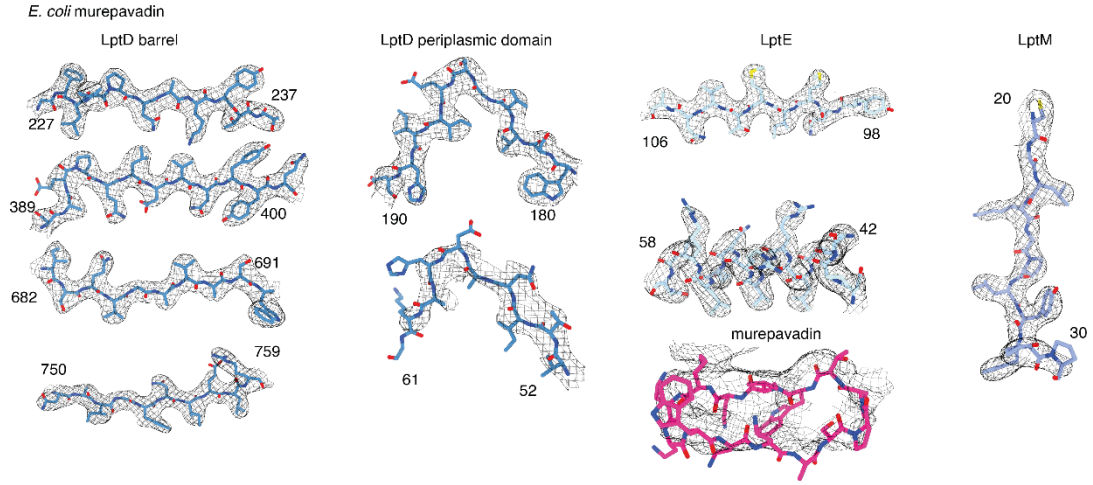

Fig. S11. Structural model of LptDEM$_{Eco}$ with murepavadin. Representative examples of each chain of the model (LptD, LptE, LptM and murepavadin) at different regions of the structures, with the first and last amino acid number labeled, shown individually within the experimentally determined cryo-EM map (grey mesh) at appropriate contour levels.

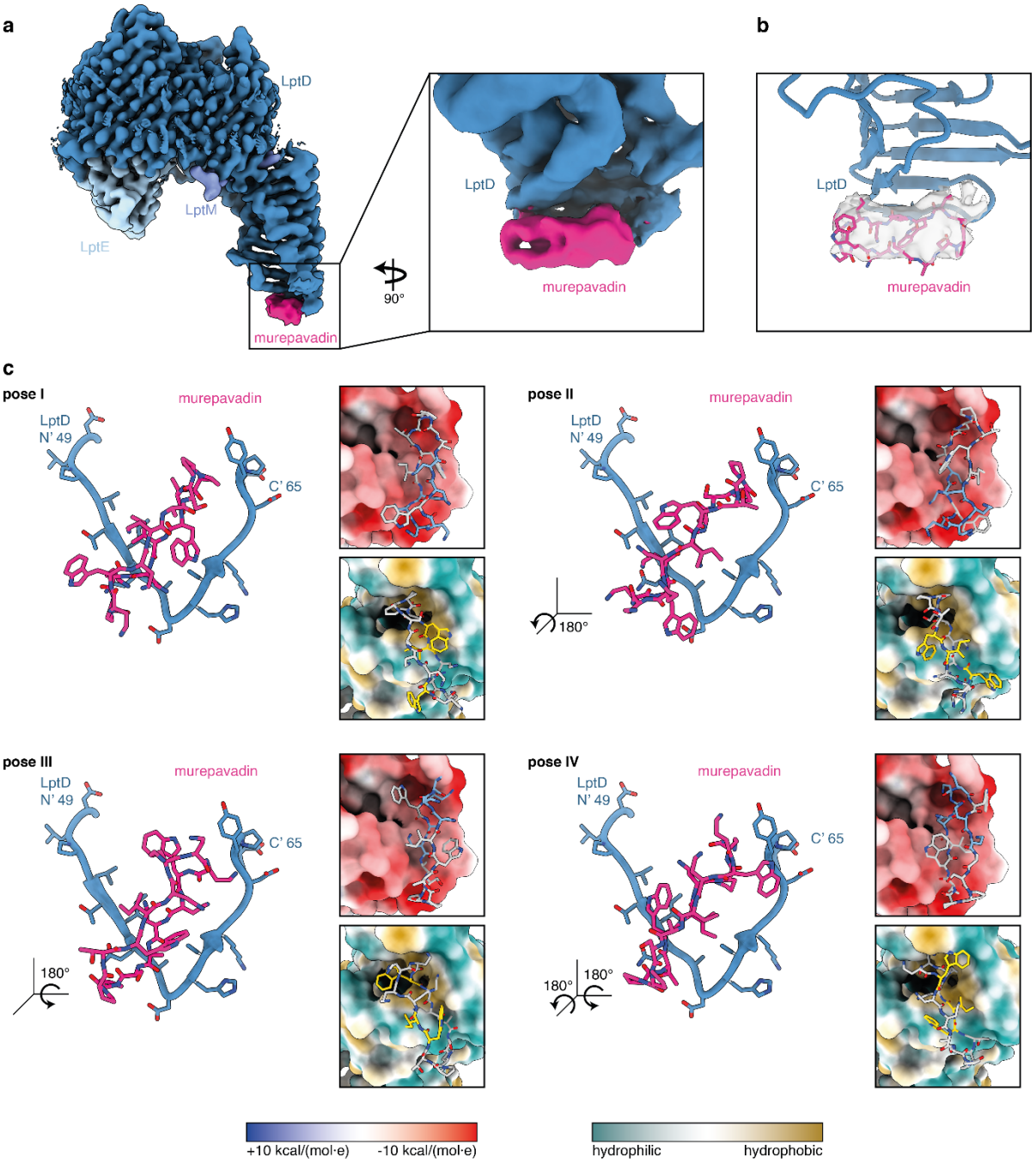

Fig. S12. Molecular poses of murepavadin binding to LptDEM$_{Eco}$. a Cryo-EM reconstructions of LptDEM$_{Eco}$–murepavadin, at representative contour levels for each subunit (LptDEM$_{Eco}$, blue; murepavadin, pink), with a close-up view of the density attributed to murepavadin. **b** Molecular model showing the possible backbone fit of murepavadin within its density (grey). **c** Bottom view of the binding site with the four formally possible poses of murepavadin (I–IV). Each pose is shown in context of electrostatics and hydrophobicity of LptD, with highlighted positively charged residues (blue) or hydrophobic residues (yellow) of murepavadin. Pose I has the best match of electrostatics and hydrophobicity, whereas II, III and IV show partial electrostatic and hydrophobic mismatch between the ligand and the protein.

Table S1.

List of primers used in the study.

Primer name	5' – 3' sequence
prJS1714	TTAATAAGGAGATATACCATGAAAAAACGTATCCCCACTCTC
prJS1715	GCGCCGAGCTCGAATTCGGATCCTCACAAAGTGTTTTGATACGGCAG
prJS1716	TATAAGAAGGAGATATACATATGCGATATCTGGCAACATTGTTGTTATCTC
prJS1717	GCGGTTTCTTTACCAGACTCGAGTCAATGATGGTGATGATGGTGGTGATGGTTACCCAGCGTGGTGGAG
prJS1976	TGACTCGAGTCTGGTAAAGAAACC
prJS2026	TAATTCTAATGAATTTAATCACTGCCCGCTTTCCAG
prJS2027	TTAAATTCATTAGAATTACTTGTCATCGTCGTCCTTGTAGTCGTAATTCACCTGGGATGGAC
prJS2028	CGTCACCGGAATAATAATATCTC
prJS2029	ATTATTATTCCGGTGACGGCGCAACGCAATTAATGTAAGTTAG
prJS2034	AAGGCCTTCCTTAGCGCGCCCTCGAGTTATCACATTGCCTGGTCCTCTC
prJS2035	CGCGCTAAGGAAGGCCTTATGAAACGTATTTTAACAAGTGCGG
prJS2093	TTATTAAGTGGGTGCAACTTAAACAAAATTATTTCTACAGGGGAATTG
prJS2094	GTTGCACCCACTTAATAAGGAGGTCAGGCCATGGCCGTCAAAAGTCTGG
prJS2097	TATGACTTACCTCCTTATCAATGATGGTGATGATGGTGG
prJS2098	GATAAGGAGGTAAGTCATATGAAAAACGTGTTTAAGGCACTC
prJS2099	TTTACCAGACTCGAGTCACTTGTCATCGTCGTCCTTGTAG

Table S2.

Cryo-EM data collection and refinement statistics.

	$LptDEM_{Eco}$ (EMDB-X) (PDB XXX)	$LptDEM_{Eco}$–thanatin (EMDB-X) (PDB XXX)	$LptDEM_{Eco}$–murepavadin (EMDB-X) (PDB XXX)	$LptDEM_{Pae}$ (EMDB-X) (PDB XXX)	$LptDEM_{Pae}$–murepavadin (EMDB-X) (PDB XXX)
Data collection and processing					
Magnification	165,000x	165,000x	165,000x	165,000x	165,000x
Voltage (kV)	300	300	300	300	300
Electron exposure (e–/Å2)	50	50	50	50	50
Defocus range (μm)	-0.6 to -2.0	-0.6 to -2.0	-0.6 to -2.0	-0.6 to -2.0	-0.6 to -2.0
Pixel size (Å)	0.73	0.73	0.73	0.73	0.73
Symmetry imposed	C1	C1	C1	C1	C1
Initial particle images (no.)	2,814,993	5,205,377	2,720,690	2,559,821	11,667,764
Final particle images (no.)	514,654	320,944	461,622	235,651	260,951
Map resolution (Å)	2.51	2.73	2.49	2.96	2.57
FSC threshold	0.143	0.143	0.143	0.143	0.143
Map resolution range (Å)	1.6–29.5	1.8–35.3	1.6–25.8	1.7–26.3	1.7–32.1
Refinement					
Initial model used	AlphaFold, *ab-initio*	AlphaFold, *ab-initio*	AlphaFold, *ab-initio*	AlphaFold, *ab-initio*	AlphaFold, *ab-initio*
Model resolution (Å)	2.7	2.9	3.1	3.2	3.2
FSC threshold	0.5	0.5	0.5	0.5	0.5
Map sharpening B factor (Å2)	104.7	107.6	103.0	112.7	95.8
Model composition					
Non-hydrogen atoms	7,445	7,613	7556	8,207	8,318
Protein residues	925	946	939	1024	1038
B factors (Å2)					
Protein	62.26	101.76	126.90	142.04	137.01
R.m.s. deviations	0.010				
Bond lengths (Å)	0.883	0.006	0.005	0.003	0.004
Bond angles (°)		0.833	0.512	0.581	0.576
Validation					
MolProbity score	0.74	0.58	1.05	0.97	1.06
Clashscore	0.76	0.20	0.95	0.97	2.09
Poor rotamers (%)	0	0.12	0.37	0.11	0.91
Ramachandran plot					
Favored (%)	98.15	98.19	96.09	98.53	97.65
Allowed (%)	1.85	1.81	3.91	1.47	2.25
Disallowed (%)	0.0	0.0	0.0	0.0	0.1

Table S3.

Alanine-scan of murepavadin with indicated MIC on three different *P. aeruginosa* strains.[a]

Pae strain	mur	T1	W2	l3	Dab4	Orn5	DDab 6	Dab7	W8	Dab9	Dab10	S12	DP13	P14
PAO1	0.06	0.06	>4	4	0.5	0.5	0.25	1	>4	1.125	1	0.075	0.185	0.12
ATCC 27853	0.03	0.03	>4	1	0.25	0.375	0.12	0.25	>4	0.12	0.5	0.045	0.09	0.06
Walter	0.03	0.045	>4	3	0.75	1	0.25	1	>4	0.5	>4	0.045	0.09	0.25

[a] Cells are colored in a green-yellow-red gradient from green = 0.03 to red = >4.